17th International Conference on Greenhouse Gas Control Technologies, GHGT-17

20th -24th October 2024 Calgary, Canada

Accelerated CO2 Storage Optimization Using Multi-Resolution Fourier Neural Operator at the Illinois Basin Decatur Project (IBDP)

Chin-Hsiang Chan[a], Masahiro Nagao[a], Akhil Datta-Gupta[a]

[a]*Texas A&M University, College Station, 77840, USA*

Abstract

Carbon capture and storage is one of the most promising methods for reducing greenhouse gases, and extensive research has been conducted to examine how to sequester CO2 into subsurface environments, such as depleted oil and gas fields and deep saline aquifers. The injection of CO2 into subsurface formations entails various risks, necessitating a comprehensive evaluation of several factors such as seismic activity, seal integrity, and CO2 leakage. Therefore, a CO2 injection project involves multiple objectives, and these objectives often exhibit trade-offs, rendering the optimization of CO2 injection challenging. Traditional multi-objective optimization requires hundreds of forward simulations, which is computationally prohibitive for large-scale field cases. In this study, we present an efficient deep learning-based workflow for CO2 injection schedule optimization during CO2 sequestration. A data-driven proxy model is developed to accelerate the optimization workflow, which makes it scalable to large-scale field applications.

Our deep learning workflow utilizes a recently developed machine learning architecture, Fourier Neural Operator (FNO), as a data-driven proxy model. The input of the proposed FNO model is composed of permeability distribution and CO2 injection schedule, and it estimates pressure and saturation distribution in the reservoir. One of the difficulties of data-driven model is the requirement of large training datasets, involving thousands of numerical simulations. By leveraging the super-resolution feature of the FNO, the model can be trained using low resolution image, and the trained model can predict high resolution image. Therefore, coarse-scale reservoir models can be used for training data generation, resulting in a significant reduction in data generation costs. In our workflow, numerical simulations are run using a coarsened permeability and porosity models with different CO2 injection schedules, which provide coarse-scale pressure and saturation distributions as training data. The FNO model is trained using the generated coarse-scale data, and the trained model can predict fine-scale pressure and saturation distributions with minimal loss of accuracy. For CO2 injection schedule optimization, a multi-objective genetic algorithm is utilized, where the FNO-based proxy model is used as a forward model. The optimization can include several different objectives, such as minimizing pressure increase in the reservoir, maximizing CO2 injection amount and storage efficiency.

The power and efficiency of our approach are demonstrated using both synthetic and field applications. We initially demonstrate the advantages of our deep learning-based workflow using a synthetic case of gas injection into an aquifer. Next, we apply our workflow to the Illinois Basin Decatur Project (IBDP), which is a large-scale CO2 injection project into deep saline aquifer in Illinois Basin, USA. For the field application, training data are generated at the coarse-scale for computational efficiency and, 90% computational time reduction is achieved compared with the fine-scale simulations. The accuracy of the trained proxy model is verified by comparing with a commercial reservoir simulator. Finally, the multi-objective optimization workflow is conducted using the FNO-based proxy model. The optimization framework has shown significant improvement across multiple objectives, achieving orders-of-magnitude faster performance compared to traditional workflows that rely on numerical simulation as a forward model.

The novelty of this work is the development of multi-resolution FNO-based fast proxy model for reservoir simulation and its application to CO2 injection schedule optimization. The use of super-resolution feature in FNO in conjunction with coarse-scale models reduces substantially the training data generation cost. The proxy model accelerates forward simulation by orders of magnitude and enables evaluation of various optimization scenarios for large-scale field cases.

Keywords: CO2 geological storage, Deep learning, Fourier neural operator, Injection optimization

1. Introduction

The Paris Agreement aims to limit global warming to below 2°C, ideally no more than 1.5°C above pre-industrial levels. As the 2018 report of the Intergovernmental Panel on Climate Change (IPCC) emphasizes, a 1.5°C to 2.0°C increase in global temperatures could have serious consequences for both human and natural systems [1]. Therefore, reducing greenhouse gas emissions is an urgent priority for current human being. Among the strategies for mitigating global warming, Carbon Capture and Storage (CCS) emerges as one of the most promising technologies. CCS technologies capture carbon dioxide (CO2) and permanently sequestrate them in subsurface geological formations. The progress of CCS deployment has not aligned with expected benchmarks [2] due to uncertainties in the assessment of storage and injection capacities that have hampered the deployment of CCS technologies. The injection of CO2 into geological formations is associated with an increase in pressure and the migration of the gaseous plume, necessitating accurate forecasts of these dynamic behaviors to evaluate various risks including seismic activity, seal integrity and CO2 leakage [3, 4].

In typical CCS operation, CO2 is injected into the subsurface space through an injection well, and the CO2 plume propagates through porous geological formations. At this point, we aim to inject largest possible amount of CO2 to maximize total CO2 storage amount in this CCS project. However, injecting CO2 into subsurface space is associated with the pressure increase which is regarding to risk of seismic event or integrity of sealing layer [3]. Large pressure rises could activate faults and cause cracks in the sealing layer. In addition, efficient utilization of the subsurface space is also an important key factor in terms of avoiding CO2 leakage or maximizing the storage capacity. This utilization efficiency is often referred to as storage efficiency of CO2 injection [4], which is basically representing the proportion of gas plume volume to the available reservoir pore volume. For optimal CCS project, considering these key factors is essential for project success.

To accurately evaluate these key factors, classical reservoir simulation is commonly utilized. However, existing numerical methods for simulating CO2-water, multiphase flow are highly computationally expensive, requiring hours or days for large-field case. This is insufficient to perform the detailed computational analysis necessary to facilitate the global implementation of CCS projects. Rapid reservoir simulations have been investigated for several decades in oil and gas industry using data-driven model or reduced-order-model, which have been successfully applied to CCS deployment in several literatures [5-8]. However, these methodologies still have some problems in applying them to large fields, such as requiring significant computational effort for preprocessing. Especially, most of machine or deep learning-based proxy model requires thousands of training data, necessitating extensive reservoir simulation runs that can offset the speed advantages of a fast proxy model.

In this work, we present an efficient deep learning-based workflow for CO2 injection schedule optimization during CO2 sequestration. To address the large training cost issues in existing deep learning-based proxy model, we have developed a multi-resolution machine-learning model that utilizes super-resolution capabilities of neural operators. The multi-resolution machine-learning model can train with coarse training data but predict at fine-scale. This multi-resolution feature allows for the use of upscaled reservoir models, substantially reducing the cost associated with generating training data. The general workflow begins with the upscaling of the reservoir model to reduce reservoir simulation costs. Subsequently, training data are generated using the upscaled model. Although hundreds of reservoir simulations are required for this process, the computational cost is significantly reduced due to the upscaling. The proposed proxy model is then trained on the generated coarse-scale data, which will provide the fine-scale predictions of reservoir dynamic properties. This data-driven proxy model accelerates the optimization workflow, making it scalable for large-scale field applications.

2. Methodology

2.1. Neural Operators

Neural operator is a class of machine learning models designed to learn mappings between infinite-dimensional function spaces. Fig. 1 shows the comparison between classical neural networks and neural operators. While classical neural networks perform points to points mapping, the neural operators perform function to function mapping. Because neural operators predict continuous functions, it can obtain the any discretized points on that predicted function. This capability is referred to as the "zero-shot super-resolution" feature [9], which means that the neural operators can perform the resolution-invariant prediction.

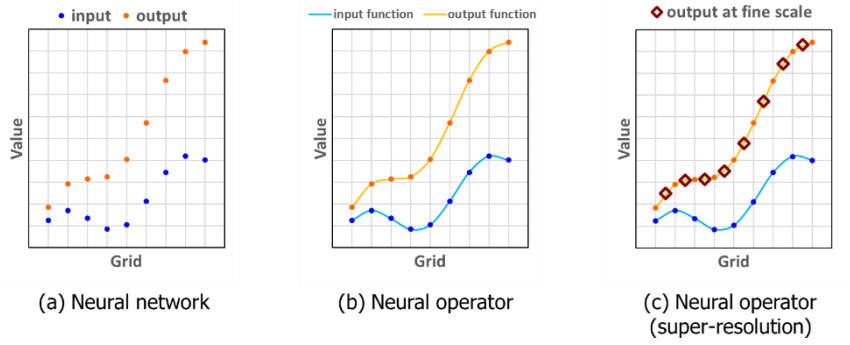

Fig. 1. Comparison between classical neural networks and neural operators. These figures are created after [10]

Neural operators utilize linear integral operation to achieve this function to function mapping while classical neural networks utilize number of linear functions [10]. The neural operators consist of the following iterative architecture.

$$v_{t+1}(x) = \sigma\left(Wv_t(x) + \int_D \kappa_\phi\big(x, y, a(x), a(y)\big)v_t(y)dy\right) \tag{1}$$

where v: functions, W: linear operator, κ: kernel function parametrized by parameter ϕ. The universal approximation theorem of this operator learning is provided in several literatures [9, 11-13]. Recently, neural operators are applied to various scientific computing problems including seismic wave propagation [14], weather forecasts [15], and CO2 sequestration problems [16].

2.2. Fourier Neural Operators (FNO)

Although the linear integral operation equips neural operators with the ability to work across multiple resolutions, the integration process is notably time-consuming in the algorithm. It is not feasible to compute this process analytically, and it still have scalability issues in practical applications. Fourier Neural Operator (FNO), proposed by Li et al. [17], addresses this challenge by approximating integral operation using fast Fourier transform. By facilitating the fast Fourier transform as described in Eq. (2), FNO significantly accelerates the computational speed of neural operators, resulting faster and more effective function to function mappings.

$$\int_D \kappa_\phi\big(x, y, a(x), a(y)\big)v_t(y)dy \approx \mathcal{F}^{-1}\left(R_\phi \cdot (\mathcal{F}v_t)\right)(x) \tag{2}$$

This approximation relies on the principle that convolution in the Fourier space corresponds to the integral operations in the original space. Consequently, FNO leverages this principle to structure its model architecture, as illustrated in Fig. 2. The FNO architecture can be described in three steps: First, it transforms the input physical

functions to Fourier basis (modes) in the Fourier space through fast Fourier transform. Next, it applies convolutions with weights of FNO model, which are calibrated during model training. Lastly, we transform the calculated output functions in the Fourier domain back into the physical domain. In addition to the convolution in Fourier space, FNO also utilizes local liner transformation in physical space as indicated in the operation W. The outputs from both the Fourier domain and physical domain are combined, and then an activation function is applied to introduce non-linearity. This process is iterated for each layer.

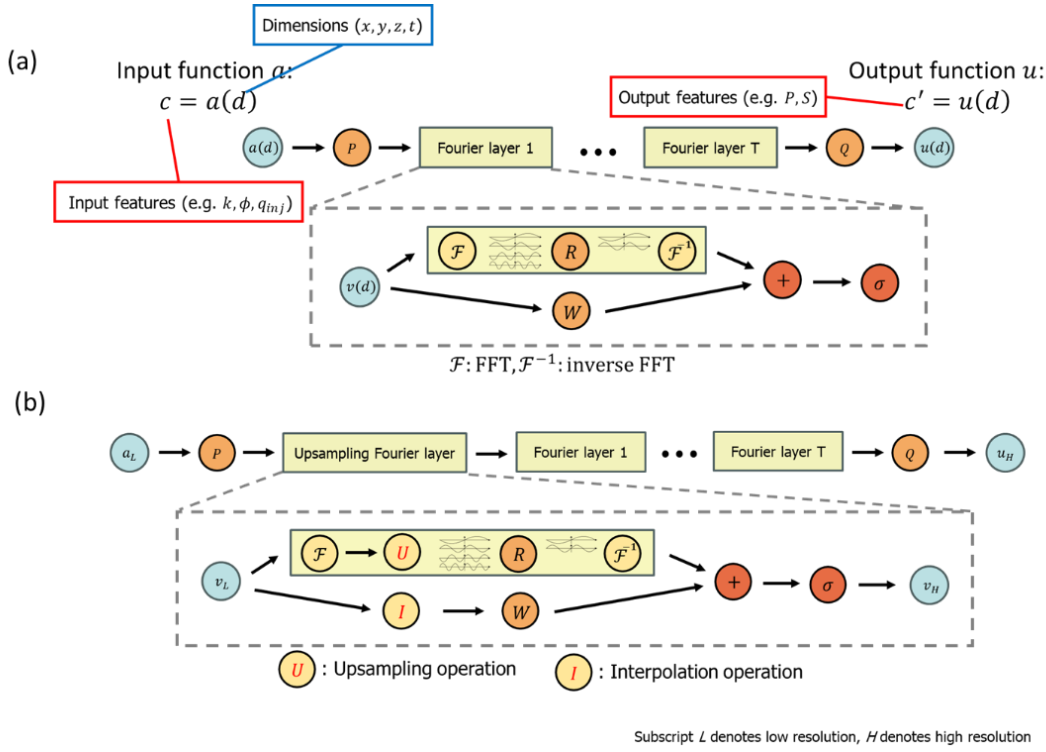

Fig. 2. Architecture of (a) Fourier Neural Operator (FNO) and (b) multi-resolution FNO

2.3. Multi-resolution Fourier Neural Operators

The multi-resolution capability of FNO has been demonstrated in a variety of studies, including oil-water two-phase flow problems [18]. However, several previous studies showed that the original FNO model had poor prediction performance for complex physics [19] including CO2 injection scenario. This issue of prediction accuracy arises when we try to predict images that has finer scales than the generated training data images.

To mitigate this issue, we updated the FNO architecture, which we call the updated FNO model as multi-resolution FNO. These modifications involve interpolation within both the physical and Fourier space, allowing the model to bridge predictions from coarse to fine scales. This strategy takes advantage of the fact that FNO provides the best forecasting performance at the resolution of generated training data images. In our algorithm, the training data is generated using upscaled reservoir model. Proposed FNO architecture is trained to predict the fine-scale output images from the coarse-scale training data images. The architecture of multi-resolution FNO is shown in Fig. 2(b) that employs "Upsampling Fourier layer" that perform interpolations.

Fig. 3 outlines the training and testing workflow for the multi-resolution FNO. The process begins with coarse input data fed into the multi-resolution FNO. The model provides fine-scale output images through internal interpolation. These fine-scale images are subsequently upscaled back to the coarse-scale to compute data misfits against the coarse training data generated by numerical simulator. Based on the data misfits, the model conducts backpropagation to compute the gradients of the loss with respect to each model weights. These weights are then

updated in the direction of the gradient, with the magnitude of the updates regulated by the learning rate. Once training is completed, the model can predict fine-scale output images from coarse input images.

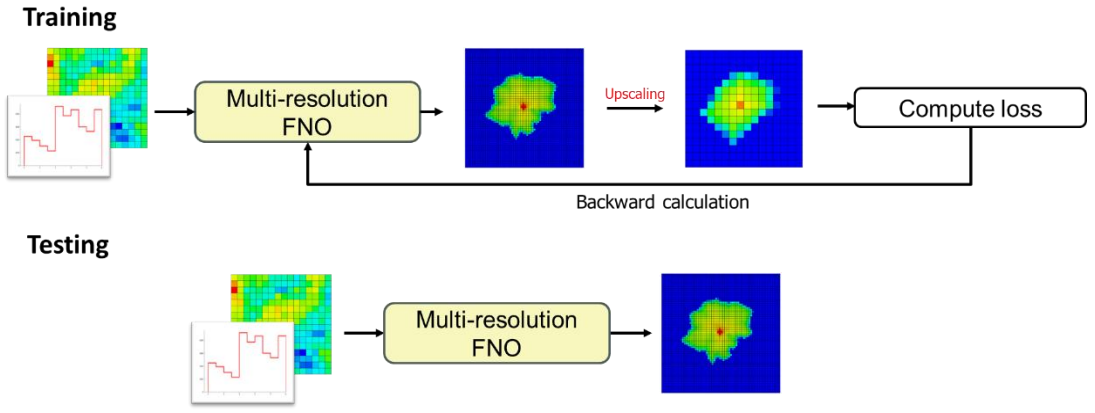

Fig. 3. Workflow of training and testing in multi-resolution FNO

2.4. Multi-objective Genetic Algorithms (MOGA)

We utilize Multi-Objective Genetic Algorithm (MOGA) to optimize CO2 injection schedule while considering multiple objective functions. The primary advantage of MOGA lies in its ability to optimize each objective function simultaneously, unlike other optimization algorithms that simply aggregate all objective functions into a single function. The conventional approach does not guarantee to improve all objectives, and it is required to tune the weights associated with each objective function. On the other hand, MOGA guarantees to improve all objective functions simultaneously. As a result of MOGA optimization, we obtain a set of optimal realizations known as the Pareto front. This approach ensures that every realization on the Pareto front is optimal, as none are dominated by others across all objectives. This guarantees that the Pareto front exclusively contains the most optimal realizations. Users can select most desirable realization based on their specific requirements within the optimized realizations.

Our MOGA software utilizes the Non-dominated Sorting Algorithm II (NSGA-II) [20], a widely recognized evolutionary algorithm for addressing multi-objective optimization challenges. The MOGA workflow begins with an initial generation, where the injection rates are randomly selected within a predefined range. Each realization is then evaluated using the FNO-based proxy model to compute the fitness in terms of objective functions. Realizations with superior objective function values are chosen as parents, and the next generation is created through crossover and mutation, which is inspired by principles of evolutionary theory. This process is repeated through several generations until convergence is achieved, resulting in an optimized set of realizations. Since MOGA produces multiple optimal solutions on the Pareto front, users can choose the most suitable realization based on specific requirements or constraints, such as target CO2 storage amount or maximum allowable pressure.

3. Validation using a 2D synthetic case

The CO2 saturation prediction performance of the proposed multi-resolution FNO model is validated by using 2D synthetic reservoir case and compared against the original FNO model. This 2D synthetic case has 64×64 uniform grid with heterogeneous permeability field. To test the prediction across the multi-resolution, the 64×64 heterogeneous permeability is upscaled to 32×32. A CO2 injection well is located at the center of both models. Training data are generated by changing CO2 injection schedule. 20 unit time intervals are defined where each interval has 30 days of time length. The injection rates in these intervals are sampled from the range between 100 to 1000 MSCF/day. 1000 samples are generated using upscaled geologic model (32×32) and data are divided into 90 % for training and 10 % for validation. The input functions are permeability, porosity, well location, injection rates and grid information (x, y, z). The output function is gas saturation in all time steps. Using these training data, original FNO and multi-resolution FNO are trained to map from input properties to output properties.

Fig. 4 compares the predictive performance of CO2 saturation between numerical simulator and these two models. Referring to the error map shown in the right column of Fig. 4, large error was observed especially around the gas saturation front in the prediction of the original FNO. This is fatal as a proxy model for CCS operation because this error impairs the accurate assessment of CO2 leakage risks. On the other hand, multi-resolution FNO provides much less prediction error. Although it still has a relatively larger error in saturation front, the magnitude is reasonably small. The relative mean square errors of these two models are 0.336 for original FNO and 0.139 for multi-resolution FNO.

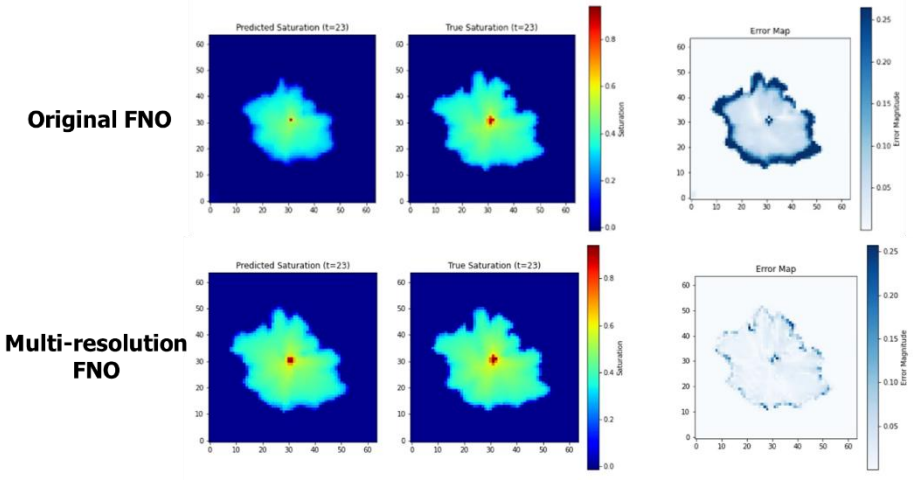

Fig. 4. Prediction performance comparison between original FNO and multi-resolution FNO. CO2 plume image provided from proxy model (left), numerical simulator (middle) and their differences (right)

4. Field Application

4.1. Model Description

The Illinois Basin – Decatur Project (IBDP) is a large-scale CCS project by the Midwest Geological Sequestration Consortium. This project involves injecting supercritical CO2 at a rate of approximately 1102 tons (1000 metric tonnes) per day for three years into the basal part of the Mt. Simon Sandstone unit [21]. Fig. 5 shows the IBDP reservoir model and satellite view of IBDP site. There are CO2 injection well (CCS1), monitoring well (VW1) and geophysical monitoring well (GM1). GM1 is shallowly drilled to obtain time-lapse 3D vertical seismic profile and micro seismic data, thus, not shown in reservoir model. The reservoir model consists of 1.73 million cells (126×125×110), structured in a tartan grid with higher resolution near the center. The model spans an area of 9.3 by 9.7 miles laterally and is situated at a depth ranging from 4250 to 7800 ft. Fig. 6 illustrates the horizontal and vertical permeability and porosity of the IBDP model. The injection zone, located in the middle layer, exhibits higher permeability and porosity. Beneath the injection zone, there is a lower permeability zone that acts as a baffle for the CO2 plume and pressure. Additionally, some small baffles are modeled by adjusting vertical permeability.

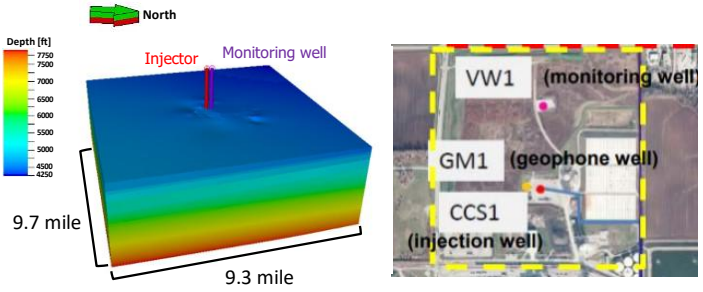

Fig. 5. IBDP reservoir model (left) and satellite view of IBDP site (right)

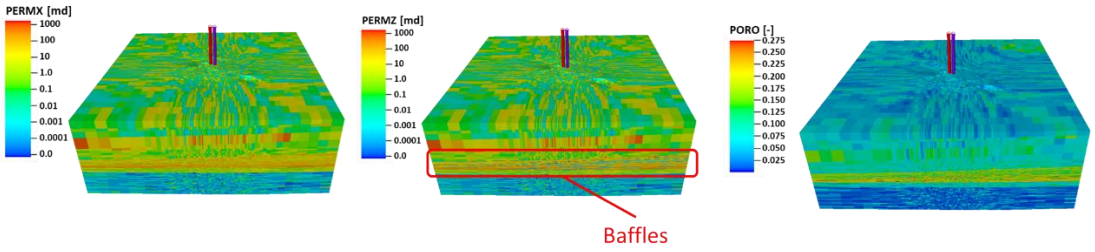

Fig. 6. Petrophysical properties in IBDP model: Horizontal permeability (left), vertical permeability (middle), porosity (right)

In this work, we utilized ECLIPSE Compositional simulation with CO2STORE option, which is compositional isothermal flow simulator designed for CCS in aquifer. CO2STORE option allows the CO2 component to exist in water phase. The IBDP model includes three components: CO2, H2O, and NaCl. A hysteresis model is applied, providing separate relative permeability tables for drainage and imbibition. During CO2 injection, the water saturation decreases, necessitating the use of the drainage relative permeability curve. However, after CO2 injection is stopped, CO2 migration occurs due to gravity or diffusion effects, and under such circumstances an imbibition curve is used. The gap between the drainage and imbibition curves facilitates the residual trapping of CO2 within the rock. The initial condition is modeled using hydrostatic equilibrium with a datum depth of 6345 feet and a datum pressure of 3205 psi. To simulate a typical aquifer reservoir, infinite-acting boundary conditions are assumed. To maintain constant pressure at the boundary, a large pore volume multiplier is applied to the side boundary cells. For the upper and bottom boundaries, no-flow boundary conditions are assumed.

4.2. Investigation of Coarsening Scheme

To fully leverage the prediction benefits of the multi-resolution capabilities of the FNO-based proxy model, optimal coarsening scheme is crucial. While the proposed multi-resolution FNO-based proxy model outperforms the original FNO, it still experiences performance degradation when tested at resolutions significantly different from those which the model was trained on. On the other hand, the extent of coarsening directly impacts the acceleration achieved in the data generation process, as it reduces the number of active cells in reservoir simulations. Therefore, the primary strategy of coarsening is to coarsen the model as much as possible while maintaining high prediction performance at the original fine scale. In this research, horizontal and vertical coarsening schemes are considered separately. Vertical coarsening is investigated considering the bias-variance trade-off, which determines the optimal upgridding based on the geological model proposed by King, et al. [22]. This approach sequentially examines the number of layers, and the heterogeneity preserved in coarsened model. More details about the vertical coarsening can be found in these references [22-24]. For horizontal coarsening, 2×2 areal coarsening is utilized which is uniformly merging every two cells into one cell in x and y directions. In other words, the 2×2 square cell is combined to single cell.

Fig. 7 shows the pressure response in wells, including injection BHP, pressure at monitoring wells (WB1 to WB3). For the 2×2×1 coarsened model, the well response is almost identical to that of the original fine-scale model. However, for the horizontal and vertical coarsened model, the error in each well response is at most 50 psi. The coarsening upscales the petrophysical properties by pore volume weighted averaging, which potentially underestimates the high permeability region such as channels. Consequently, the pressure rise starts more quickly compared to the original well response. The IBDP model is highly heterogeneous in the vertical direction, making this phenomenon particularly noticeable with vertical coarsening. Consequently, 2×2×1 coarsening is utilized throughout this work. Multi-resolution FNO could potentially address the errors associated with the vertical upscaled model. Therefore, the use of the vertical upscaled model remains a topic for future work. Fig. 7 also shows the comparison of CPU time required for single numerical simulation, demonstrating that the coarsened model reduces simulation costs more than an order of magnitude. While the number of active cells is reduced by 75 % in 2×2×1 coarsened model and 90 % in SWIFT coarsened model, more acceleration is obtained with respect to CPU time. This is likely because the reservoir simulation achieves faster convergence because of the smaller number of variables, which reduces the number of matrix calculations and significantly reduces the required computational time.

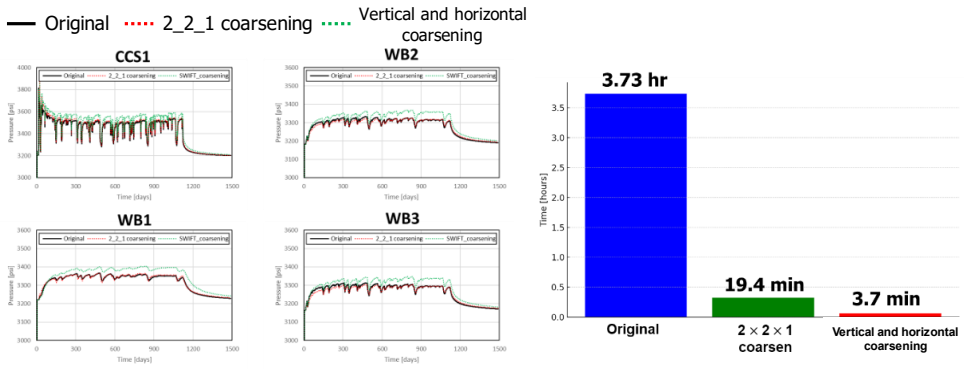

Fig. 7. Pressure responses at injector and monitoring wells (left) and comparison of CPU time required for single simulation (right)

4.3. Training Data Generation and Training of FNO-based Proxy Model

To construct the multi-resolution FNO-based proxy model, 500 realizations were created by changing CO2 injection schedules. To effectively reduce the data generation costs, coarsening is applied to the reservoir model. The model before and after coarsening is shown in Fig. 8(a). An order of magnitude speed up is achieved by this coarsening. After completing the simulations, the simulated static and dynamic reservoir properties are extracted and used as training data. In this application, the training data comprises 4D data, encompassing 3D spatial dimensions plus the time domain. Including the complete 4D data of the entire model is not feasible for a standard computer due to memory limitations. To this end, we have defined the following area of interest. Since the IBDP model is designed for CO2 sequestration in a deep saline aquifer, its boundary condition is configured to act as nearly infinite. Hence, the CO2 plume will not distribute throughout the entire reservoir, as depicted in Fig. 8(b). The area of interest is defined to capture the entire CO2 plume, and the simulation results within this region are utilized as training data. The proxy model predicts the dynamic properties within this defined area. In this work, permeability field, CO2 injection schedule, and grid coordinate information are used as input function data. Gas saturation and pressure increases are used as output function data.

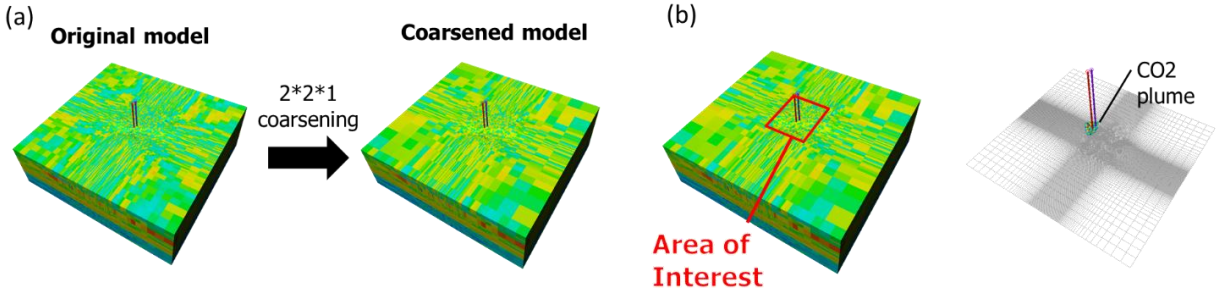

Fig. 8. Coarsened IBDP model and defined area of interest

Multi-resolution FNO was trained with T4 GPU in Google Colaboratory. Training the model takes approximately 20 minutes per epoch, and our investigations indicate that proper number of epochs to achieve loss convergence lies between 20 and 40. It should be noted that the calculated loss during the FNO training is the error against the upscaled model. To validate the prediction performance in the original fine scale, the trained proxy model was compared against a commercial numerical simulator, ECLIPSE Compositional Simulator (E300), at original fine scale. Fig. 9 depicts the comparison between two models, showing good agreement between them in terms of both gas saturation and pressure increase. The proxy model provides less continuous figure since the model is pure data-riven, which does not account for physical continuity. However, it still has good enough prediction performance, as the mean absolute errors are 0.89 for gas saturation and 3.38 for relative pressure increases which is normalized pressure increases. The trained

proxy model can make forward estimation with this accuracy in 11.5 seconds while fine scale simulation requires about 3.8 hours.

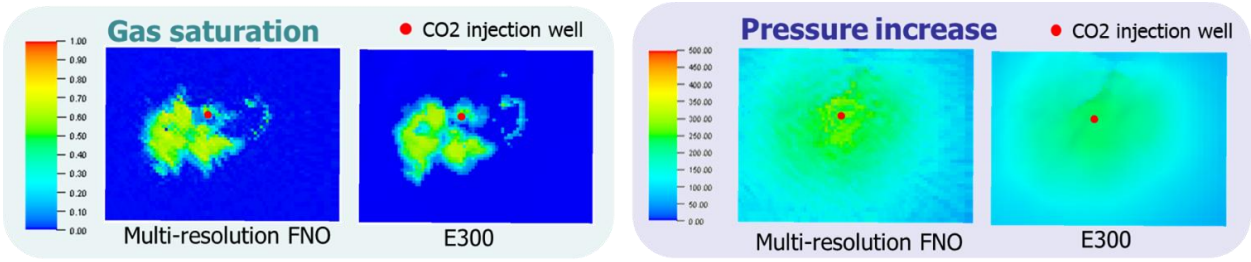

Fig. 9. Comparison between multi-resolution FNO and E300 in gas saturation and pressure increase

4.4. CO2 Injection Schedule Optimization with Multiple Objectives

Utilizing developed proxy model, MOGA is applied to IBDP model to optimize its well control for CO2 sequestration operations. In this work, the following three objective functions are employed: maximizing CO2 storage amount, maximizing sweep efficiency, and minimizing average pressure increases. Sweep efficiency is a ratio of gas volume to the CO2 footprint volume, which is the areal extent of the CO2 plume [3]. Higher sweep efficiency leads to a smaller footprint, which in turn reduces the risk of leakage and allows for more efficient utilization of subsurface space.

To optimize the CO2 injection schedule, the entire injection period is divided into 10 equal time intervals, with the injection rates in each interval optimized. Over the 500-day period, the injection rates are adjusted within a range of 10,000 to 50,000 [MSCF/day]. MOGA is performed with 15 generations and a population size of 40. In a genetic algorithm, each cycle of optimization is called a generation, and within each generation, a specified number of realizations, referred to as the population, are processed. Therefore, this optimization involved approximately 600 forward simulations. Utilizing the proxy model, two orders of magnitude speed up is achieved, where it took only 4 hours for the entire optimization workflow. Fig. 10(a) presents the results of the multi-objective optimization, displaying all realizations on a 3D axis, with each axis representing an individual objective function. Population from different generation is represented by different color and we can observe that as generation increases, the population become closer to the ideal points at the right upper corner. Since the MOGA generates the next generation considering population diversity, all subsequent generation do not always converge towards the ideal point. This phenomenon can be observed in Fig. 10(a), where some populations in larger generations remain distant from the ideal point. This characteristic is deliberately implemented to prevent the algorithm from getting stuck in local optima, thereby enhancing its ability to search for the global optimum. Consequently, we obtained more diverse populations as shown in Fig. 10(b). Because three objective functions have strong trade-off, it is not guaranteed that each realization in the pareto front simultaneously improve all three objectives. However, MOGA provided superior realizations within the Pareto front compared to the other realizations, in which users can select the most desirable realization based on their specific requirements.

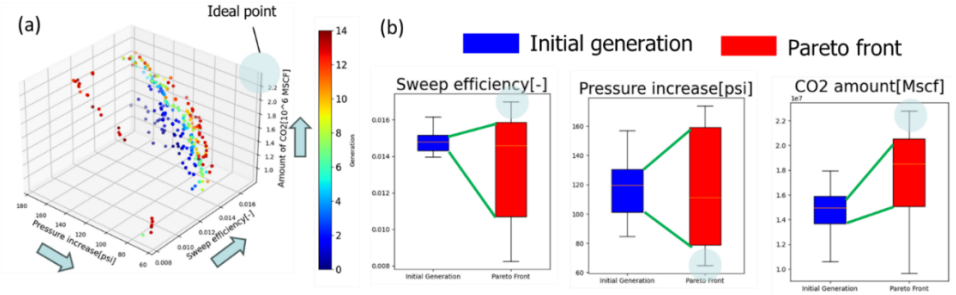

Fig. 10. Result of MOGA in 3D axis (left) and distribution changes from initial generation to pareto front (right)

Next, we validate the optimized cases using numerical simulator. The objective function evaluated during MOGA workflow is provided by FNO-based proxy model which contains the prediction errors. Hence, a numerical simulator is used to accurately evaluate the performance of the optimized case. For better interpretation, a 2D plot with CO2 amount and pressure increase is created. For comparison, a base case is prepared which is constant injection scenario. From the pareto front in Fig. 11(a), an optimized case is selected, and their injection schedules are also provided above the 2D plot. Reservoir simulations for these two cases are performed using a commercial simulator (E300). These results are shown in Fig. 11(b), where we can observe a slightly larger CO2 plume and clearly smaller pressure in the optimized case compared to the base case.

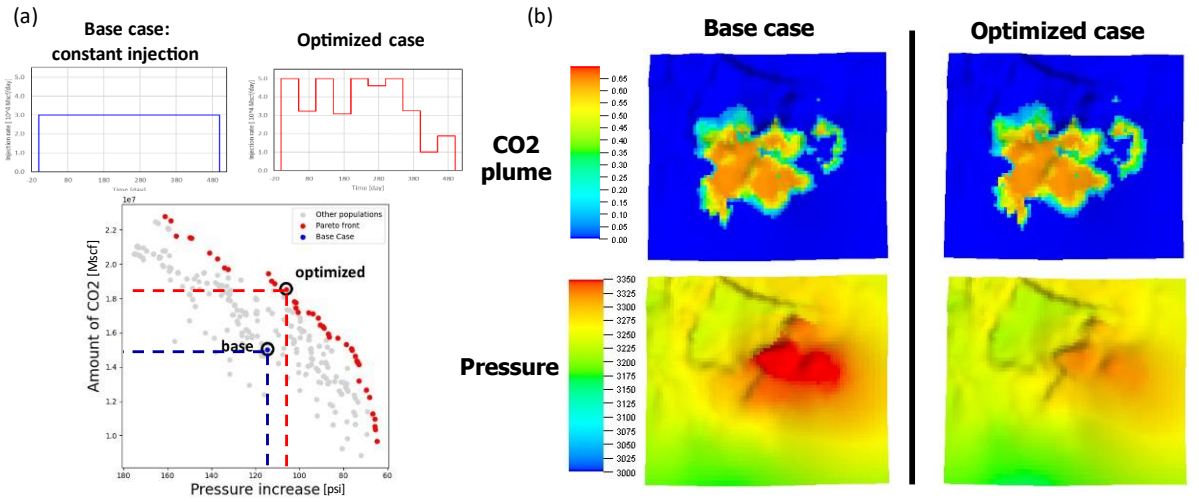

Fig. 11. Base and optimized case in 2D plots (left) and the reservoir simulation result of these cases (right)

4.5. Rate Allocation Optimization

In the previous application, the CO2 injection rate was adjusted only with the constraints of the maximum and minimum injection rate, without considering the CO2 supply limitations. However, in a typical CCS project, CO2 injection site is designed to handle a predefined total amount of CO2, which is sourced from a nearby power plant. Therefore, it is more practical to fix the total CO2 storage volume and assign that volume to each time interval than to vary the injection rate without constraints on the total CO2 storage volume. As a result, the optimization settings are updated as follows. The optimization variables are the same as before, the injection rates at 10 time intervals, but in addition to the existing constraints of maximum and minimum injection rates, a constraint of total CO2 storage is added. This optimization task is to allocate the injection rate between interval to interval. The variation of the injection schedule affects the CO2 storage performance as shown in previous literature [25]. In this case, MOGA is performed with 10 generations and a population of 40, which is fewer generations than that in the previous case. This is because this scenario involves a two-objective optimization, whereas the previous one involved three objectives. Consequently, the optimization problem is relatively simpler and should converge more quickly, therefore, the number for generation is reduced from 15 to 10. Since the number of optimization variables remains the same, the population size is also kept the same.

Fig. 12(a) shows the result of two-objective optimization where we can see MOGA successfully optimizes the CO2 injection schedule while considering two-objective. Same as previous application, the optimized case is selected to compare with base case. These two cases are evaluated using a commercial simulator (E300). Fig. 12(b) shows result CO2 plume and pressure after injection. Similar to the previous optimized results, optimized case has slightly larger CO2 plume while it has smaller reservoir pressure. One observation is that Fig. 12 has smaller pressure than Fig. 11. This is because the three-objective optimization case includes the maximizing the CO2 storage amount, while this two-objective optimization case does not. The amount of CO2 stored in the previously optimized case is approximately

1.016 Mt, which is greater than the 0.824 Mt observed in the current optimized case; consequently, a lower pressure is noted in this scenario. In this research, rate allocation optimization across time intervals is demonstrated. However, this application requires that CO2 be stored in surface facilities to inject CO2 at the desired time interval. A future topic being considered is the optimization of injection rates across multiple zones, which would determine the CO2 injection rate for each injection zone. This approach would eliminate the need for CO2 storage at the surface, making it a more viable solution.

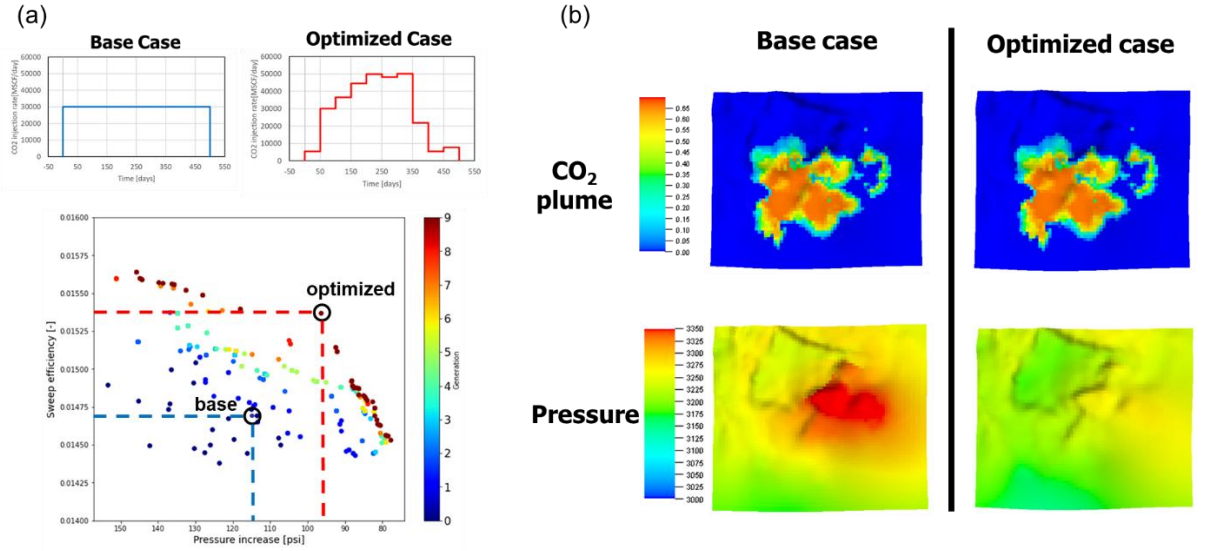

Fig. 12. Base and optimized case in two-objective optimization (left) and the reservoir simulation result of these cases (right)

5. Conclusion

We have developed a fast and efficient optimization workflow for CO2 injection schedule optimization. Our proposed approach is applied to the IBDP field case. The injection schedule of IBDP model is successfully optimized considering multiple objective functions simultaneously.

- A multi-resolution machine learning model has been developed to train with upscaled training data while predicting at the fine scale. This model is based on Fourier Neural Operators, with modifications made to enhance prediction across multiple resolutions. The performance of the developed model has been validated in a 2D synthetic case, demonstrating superior CO2 saturation predictive accuracy compared to the original FNO.
- The trained FNO proxy model can perform forward estimations in around 11 seconds, significantly accelerating the optimization workflow. The multi-resolution capability of the FNO allows for the use of a upscaled model to generate the training data, leading to a simulation cost reduction of 90%. The trained model has been subsequently validated in a commercial reservoir simulator at the original fine scale.
- Using MOGA, the CO2 injection schedule has been optimized in IBDP field case. This optimization considers three objective functions: maximizing CO2 storage amount, maximizing sweep efficiency, and minimizing pressure increase. MOGA effectively optimizes well control by improving each objective function and provides multiple optimized cases along the Pareto front. Engineers can select injection schedules from the Pareto front based on their specific situations and constraints, such as target CO2 storage amounts or maximum allowable pressure increases. The optimized case has been validated through a numerical simulator, revealing a smaller CO2 plume and lower pressure increases.
- Rate allocation optimization is also investigated. This optimization is two-objective optimization with fixed CO2 injection amount. The proposed approach successfully optimizes the allocation of CO2 injection between interval to interval.

Acknowledgements

This work is partly supported by the U.S. Department of Energy initiative on Science Informed Machine Learning for Accelerating Real Time Decisions for Subsurface Applications (SMART) and Texas A&M Joint Industry Project, Model Calibration and Efficient Reservoir Imaging (MCERI).

Disclaimer

References

[1] IPCC, "Global Warming of 1.5 ºC," 2018. [Online]. Available: https://www.ipcc.ch/sr15/
[2] E. Martin-Roberts, V. Scott, S. Flude, G. Johnson, R. S. Haszeldine, and S. Gilfillan, "Carbon capture and storage at the end of a lost decade," *One Earth,* vol. 4, no. 11, pp. 1569-1584, 2021/11/19/ 2021, doi: https://doi.org/10.1016/j.oneear.2021.10.002.
[3] S. Bachu, "Review of CO2 storage efficiency in deep saline aquifers," *International Journal of Greenhouse Gas Control,* vol. 40, pp. 188-202, 2015/09/01/ 2015, doi: https://doi.org/10.1016/j.ijggc.2015.01.007.
[4] J. T. Birkholzer, C. M. Oldenburg, and Q. Zhou, "CO2 migration and pressure evolution in deep saline aquifers," *International Journal of Greenhouse Gas Control,* vol. 40, pp. 203-220, 2015/09/01/ 2015, doi: https://doi.org/10.1016/j.ijggc.2015.03.022.
[5] Y. Zhu and N. Zabaras, "Bayesian deep convolutional encoder–decoder networks for surrogate modeling and uncertainty quantification," *Journal of Computational Physics,* vol. 366, pp. 415-447, 2018/08/01/ 2018, doi: https://doi.org/10.1016/j.jcp.2018.04.018.
[6] Z. L. Jin and L. J. Durlofsky, "Reduced-order modeling of CO2 storage operations," *International Journal of Greenhouse Gas Control,* vol. 68, pp. 49-67, 2018/01/01/ 2018, doi: https://doi.org/10.1016/j.ijggc.2017.08.017.
[7] A. Khanal and M. F. Shahriar, "Physics-Based Proxy Modeling of CO2 Sequestration in Deep Saline Aquifers," *Energies,* vol. 15, no. 12, p. 4350, 2022. [Online]. Available: https://www.mdpi.com/1996-1073/15/12/4350.
[8] G. Wen, C. Hay, and S. M. Benson, "CCSNet: A deep learning modeling suite for CO2 storage," *Advances in Water Resources,* vol. 155, p. 104009, 2021/09/01/ 2021, doi: https://doi.org/10.1016/j.advwatres.2021.104009.
[9] N. Kovachki, S. Lanthaler, and S. Mishra, "On universal approximation and error bounds for Fourier Neural Operators," p. arXiv:2107.07562doi: 10.48550/arXiv.2107.07562.
[10] K. Azizzadenesheli, N. Kovachki, Z. Li, M. Liu-Schiaffini, J. Kossaifi, and A. Anandkumar, "Neural Operators for Accelerating Scientific Simulations and Design," p. arXiv:2309.15325doi: 10.48550/arXiv.2309.15325.
[11] C. Tianping and C. Hong, "Universal approximation to nonlinear operators by neural networks with arbitrary activation functions and its application to dynamical systems," *IEEE Transactions on Neural Networks,* vol. 6, no. 4, pp. 911-917, 1995, doi: 10.1109/72.392253.
[12] K. Bhattacharya, B. Hosseini, N. B. Kovachki, and A. M. Stuart, "Model Reduction and Neural Networks for Parametric PDEs," p. arXiv:2005.03180doi: 10.48550/arXiv.2005.03180.
[13] S. Lanthaler, S. Mishra, and G. E. Karniadakis, "Error estimates for DeepOnets: A deep learning framework in infinite dimensions," p. arXiv:2102.09618doi: 10.48550/arXiv.2102.09618.
[14] Y. Yang, A. F. Gao, J. C. Castellanos, Z. E. Ross, K. Azizzadenesheli, and R. W. Clayton, "Seismic Wave Propagation and Inversion with Neural Operators," *The Seismic Record,* vol. 1, no. 3, pp. 126-134, 2021, doi: 10.1785/0320210026.
[15] J. Pathak *et al.*, "FourCastNet: A Global Data-driven High-resolution Weather Model using Adaptive Fourier Neural Operators," p. arXiv:2202.11214doi: 10.48550/arXiv.2202.11214.
[16] G. Wen, Z. Li, Q. Long, K. Azizzadenesheli, A. Anandkumar, and S. M. Benson, "Real-time high-resolution CO$_2$ geological storage prediction using nested Fourier neural operators," p. arXiv:2210.17051doi: 10.48550/arXiv.2210.17051.
[17] Z. Li *et al.*, "Fourier Neural Operator for Parametric Partial Differential Equations," p. arXiv:2010.08895doi: 10.48550/arXiv.2010.08895.
[18] K. Zhang *et al.*, "Fourier Neural Operator for Solving Subsurface Oil/Water Two-Phase Flow Partial Differential Equation," *SPE Journal,* vol. 27, no. 03, pp. 1815-1830, 2022, doi: 10.2118/209223-PA.
[19] M. A. Rahman *et al.*, "Pretraining Codomain Attention Neural Operators for Solving Multiphysics PDEs," p. arXiv:2403.12553doi: 10.48550/arXiv.2403.12553.
[20] K. Deb, A. Pratap, S. Agarwal, and T. Meyarivan, "A fast and elitist multiobjective genetic algorithm: NSGA-II," *IEEE Transactions on Evolutionary Computation,* vol. 6, no. 2, pp. 182-197, 2002, doi: 10.1109/4235.996017.
[21] R. A. Bauer, M. Carney, and R. J. Finley, "Overview of microseismic response to CO2 injection into the Mt. Simon saline reservoir at the

Illinois Basin-Decatur Project," *International Journal of Greenhouse Gas Control,* vol. 54, pp. 378-388, 2016/11/01/ 2016, doi: https://doi.org/10.1016/j.ijggc.2015.12.015.

[22] M. J. King *et al.*, "Optimal Coarsening of 3D Reservoir Models for Flow Simulation," *SPE Reservoir Evaluation & Engineering,* vol. 9, no. 04, pp. 317-334, 2006, doi: 10.2118/95759-pa.

[23] S. Du, "Multiscale reservoir simulation: Layer design, full field pseudoization and near well modeling," Ph.D., Texas A&M University, United States -- Texas, 3537240, 2012.

[24] I. Syed, C.-H. Liu, M. G. Kelkar, and M. J. King, "Improved Distance Based Upgridding and Diffuse Source Upscaling for High Resolution Geologic Models," in *SPE Annual Technical Conference and Exhibition*, 2020, vol. Day 4 Thu, October 29, 2020, D041S050R006, doi: 10.2118/201727-ms. [Online]. Available: https://doi.org/10.2118/201727-MS

[25] H. Singh, "Impact of four different CO2 injection schemes on extent of reservoir pressure and saturation," *Advances in Geo-Energy Research,* vol. 2, no. 3, pp. 305-318, 2018, doi: 10.26804/ager.2018.03.08.